9-1-2016

NPT088 reduces both amyloid-b and tau pathologies in transgenic mice

Jonathan M. Levenson

Sally Schroeter

Jenna C. Carroll

Valerie Cullen

Eva Asp

See next page for additional authors

Authors

Jonathan M. Levenson, Sally Schroeter, Jenna C. Carroll, Valerie Cullen, Eva Asp, Ming Proschitsky, Charlotte H.Y. Chung, Sharon Gilead, Muhammad Nadeem, Hemraj B. Dodiya, Shadiyat Shoaga, Elliott J. Mufson, Haim Tsubery, Rajaraman Krishnan, Jason Wright, Beka Solomon, Richard Fisher, and Kimberley S. Gannon

Alzheimer's & Dementia: Translational Research & Clinical Interventions 2 (2016) 141-155

Featured Article

NPT088 reduces both amyloid-β and tau pathologies in transgenic mice

Jonathan M. Levenson[a,*], Sally Schroeter[a], Jenna C. Carroll[a], Valerie Cullen[a], Eva Asp[a], Ming Proschitsky[a], Charlotte H.-Y. Chung[a], Sharon Gilead[a], Muhammad Nadeem[b,1], Hemraj B. Dodiya[b], Shadiyat Shoaga[b], Elliott J. Mufson[b,1], Haim Tsubery[a], Rajaraman Krishnan[a], Jason Wright[a], Beka Solomon[c], Richard Fisher[a], Kimberley S. Gannon[a]

[a]*NeuroPhage Pharmaceuticals, Inc., Cambridge, MA, USA*
[b]*Department of Neurological Sciences, Rush University Medical Center, Chicago, IL, USA*
[c]*Department of Molecular Microbiology and Biotechnology, Tel Aviv University, Tel Aviv, Israel*

Abstract

Introduction: Alzheimer's disease (AD) is characterized by appearance of both extracellular senile plaques and intracellular neurofibrillary tangles, comprised of aggregates of misfolded amyloid-β (Aβ) and hyper-phosphorylated tau, respectively. In a previous study, we demonstrated that g3p, a capsid protein from bacteriophage M13, binds to and remodels misfolded aggregates of proteins that assume an amyloid conformation. We engineered a fusion protein ("NPT088") consisting of the active fragment of g3p and human-IgG_1-Fc.

Methods: Aged Tg2576 mice or rTg4510 mice received NPT088 weekly via IP injection. Cognitive and/or functional motor endpoints were monitored during dosing. Pathology was quantified biochemically and immunohistochemically.

Results: NPT088-lowered Aβ plaque and improved cognitive performance of aged Tg2576 mice. Moreover, NPT088 reduced phospho-tau pathology, reduced brain atrophy, and improved cognition in rTg4510 mice.

Discussion: These observations establish NPT088 as a novel therapeutic approach and potential drug class that targets both Aβ and tau, the hallmark pathologies of AD.

Keywords: GAIM; General amyloid interaction motif; Novel object recognition; Spontaneous alternation; Limb clasping; Thioflavin S; Brain weight; Cerebrospinal fluid; Phospho-tau

1. Background

Alzheimer's disease (AD) is a progressive neurodegenerative disorder defined by dementia and the presence of extracellular plaques and intracellular neurofibrillary tangles, which are comprised of aggregates containing misfolded Aβ and tau, respectively [1,2]. Current therapeutic approaches for AD target one of these two protein aggregates. Most clinical trials testing the efficacy of Aβ immunization have not demonstrated significant functional improvements in patients [3–7]. Moreover, compounds targeting tau aggregation are still too early in clinical development to determine whether an approach specifically directed at tau aggregates will be efficacious [8,9].

Based on the clinical failures using Aβ immunization and animal model studies, it is postulated that therapeutic

J.M.L., S.S., J.C.C., V.C., E.A., M.P., C.C., S.G., H.T., R.K., J.W., R.F., and K.S.G. are employees of NeuroPhage Pharmaceuticals. E.J.M. and M.N. are consultants of NeuroPhage. B.S. is a scientific founder of NeuroPhage Pharmaceuticals.

[1]Current Address: Department of Neurobiology, Barrow Neurological Institute, St. Joseph's Hospital and Medical Center, Phoenix, AZ 85013.

*Corresponding author. Tel.: +1-617-945-9763; Fax: +1-617-714-5469.
E-mail address: jlevenson@neurophage.com

http://dx.doi.org/10.1016/j.trci.2016.06.004

strategies for binding and subsequent clearing of Aβ aggregates should ideally exhibit high-affinity binding to aggregated forms of the misfolded proteins (i.e., oligomers, fibers, or plaques) while sparing monomeric or native species [10,11]. In support of this hypothesis, phase I results from the ongoing PRIME clinical trial of aducanumab, a monoclonal antibody (mAb) that specifically targets aggregated Aβ, demonstrated significant reduction of Aβ plaque by PET imaging associated with significant cognitive improvement [12]. Although these results are promising and suggest that treatment with Aβ-directed therapeutics could alter AD progression, the patient population enrolled was specifically selected to exhibit a mild form of the disease, and measurements of changes in tau aggregate loads, which correlate more closely with cognitive function, were not reported. Here, we propose a therapeutic approach for AD that broadly targets aggregates of both Aβ and tau but without affecting their respective monomeric forms.

It was previously reported that the filamentous bacteriophage M13 (M13) improves cognition and decreases Aβ plaque loads in APP-overexpressing transgenic mice after chronic administration [13]. Further research to understand the mechanism of this anti-amyloid activity revealed that M13 binds to and remodels multiple types of misfolded protein aggregates in vitro, including Aβ, tau, and α-synuclein, without binding to monomeric forms of these proteins [14], and that M13 targeting of misfolded protein aggregates is mediated by a two-domain fragment of the phage capsid protein g3p. Therefore, g3p functions as a general amyloid interaction motif (GAIM), targeting multiple misfolded proteins. A fusion protein, NPT088, was engineered that consists of the active fragment of g3p and human-IgG_1-Fc

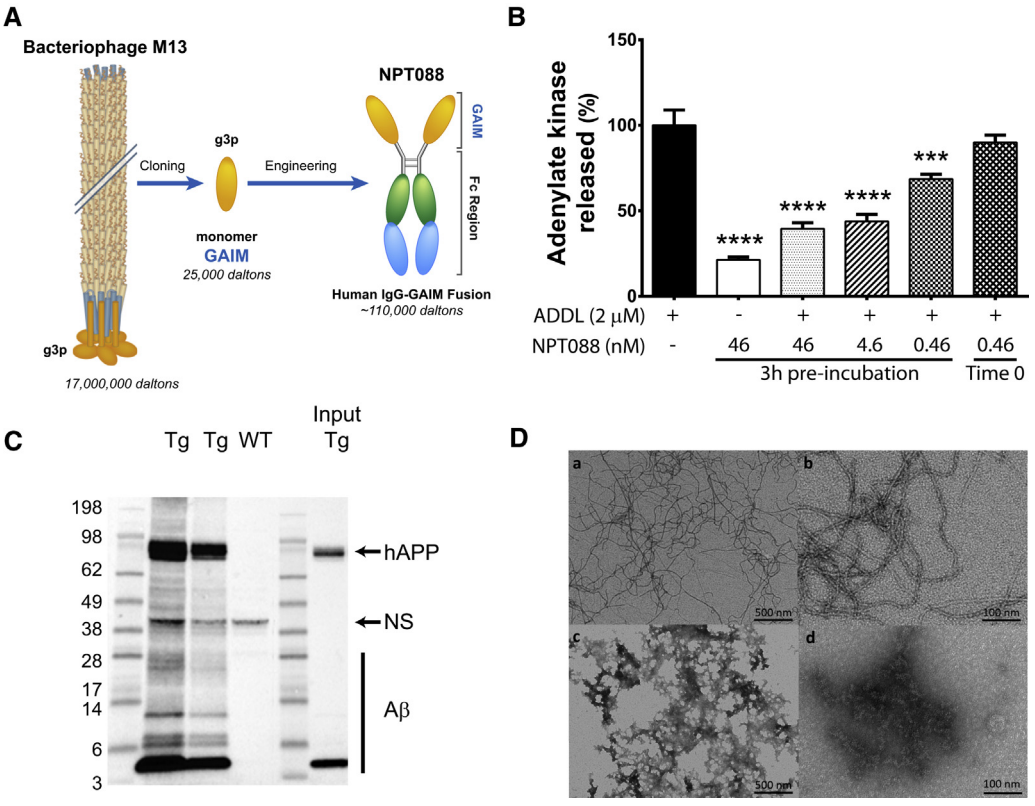

Fig. 1. Generation and in vitro characterization of NPT088, an immunoglobulin-GAIM fusion protein. (A) Native bacteriophage M13 potently and broadly binds to and disrupts a variety of misfolded protein assemblies, including Aβ, tau, α-synuclein, and yeast prion Sup35. M13, owing to its large size (17 MDa), represents a significant hurdle for effective CNS drug delivery. Subsequent characterization of amyloid fiber binding and remodeling of M13 revealed that the minor capsid protein, gene 3 protein (g3p), is critical for this activity and, furthermore, that the two N-terminal domains of g3p facilitate binding and disruption of amyloids as a general amyloid interaction motif (GAIM). The engineered fusion protein, NPT088 (NPT088), consists of the active fragment of g3p and human-IgG_1-Fc. (B) Incubation of differentiated N2a cells with 2 μM (9 μg/mL) $Aβ_{42}$ ADDLs for 24-hour-induced robust cytotoxicity. Preincubation of ADDLs with NPT088 for 3 hours significantly inhibited cytotoxicity. Co-application of ADDL and NPT088 (Time 0 control) had no effect on induction of cytotoxicity. Asterisks indicate significant difference from ADDL alone (Dunnett's test, $^{***}P < .001$, $^{****}P < .0001$). (C) NPT088 was used to precipitate Aβ from formic acid lysates of aged Tg2576 brain. Precipitates were resolved on SDS-PAGE and western blots probed with a monoclonal anti-Aβ antibody (6E10). NPT088 precipitated Aβ from formic acid extracts of brain prepared from two different Tg2576 mice (Tg). No Aβ was extracted from lysates prepared from WT mice. NS indicates nonspecific band that is present in formic acid extracts from WT brains and is recognized by 6E10. hAPP represents human amyloid precursor protein. Note the enrichment of all species of Aβ in the immunoprecipitated lanes relative to the Input material lane. (D) Transmission electron microscopy images of $Aβ_{42}$ fiber preparations incubated for 7 days and stained with 1% uranyl acetate. (a–b) Examples of Aβ fiber structure after incubation for 7 days in buffer alone. (c–d) Examples of $Aβ_{42}$ fiber structure after incubation with NPT088 (0.25 μM) for 7 days. Note the dramatic loss of fiber structure.

[14] (Fig. 1A), which has physical properties suitable for systemic administration. Here, in vivo data are presented that support the development of NPT088 as a clinical candidate for the treatment of AD.

2. Methods

2.1. Cytotoxicity assay

ADDL (Aβ42-derived diffusible ligands) assembled from $A\beta_{42}$ peptides was prepared as described in [15]. Briefly, $A\beta_{42}$ peptide (0.225 mg/mL or 50 μM) was dissolved in cold F12 medium without phenol red and refrigerated (4–8°C) for 24 hours. The resulting ADDL preparations were spun at 14,000× g for 15 minutes to remove any fibrillar material and then directly used for cytotoxicity assays. SEC analysis (Superdex 75 HR) of this preparation confirmed that $A\beta_{42}$ peptides assemble into oligomeric aggregates that range in size between 17 kDa and 70 kDa (data not shown).

N2a cells (5000 cells/well) were serum starved for 48 hours to induce differentiation. Cytotoxicity was induced via incubation with (ADDL, 2 μM or 9 μg/mL) for 24 hours. Cytotoxicity was assessed by quantifying the amount of the cytosolic enzyme adenylate kinase released into the media. Prevention of cytotoxicity was assessed by pre-incubation of ADDL preparations with NPT088 for 3 hours before application to cells. Data were analyzed by 1-way ANOVA, and post-hoc comparisons were made with Dunnett test. P value was set at $\leq .05$.

2.2. $A\beta_{42}$ fiber remodeling

$A\beta_{42}$ fiber preparations (2.5 μM) were made as previously described [14]. Fiber preparations were incubated for 7 days with either buffer alone or with NPT088 (0.25 μM). After incubation, $A\beta_{42}$ fiber preparations were stained with 1% uranyl acetate, prepared for electron microscopy, and visualized with transmission electron microscopy.

2.3. Transgenic mice

Tg2576 [16] mice purchased from Taconic (Model 1349, mixed C57Bl6/SJL background) and bi-transgenic rTg4510 [17] mice (FVB/N and 129S6 background) were bred in-house. Mice were maintained on a 12:12 light:dark cycle, and food (LabDiet, Purina) and water were provided ad libitum. In experiments that involved repeated, weekly dosing with NPT088, all mice in each treatment group, including phosphate buffered saline (PBS) control animals, were immunologically tolerized by an intraperitoneal (IP) injection of 0.5 mg of monoclonal rat anti-mouse CD4 (eBioscience, Clone GK1.5, #16-0041) 24 hours before the first dose of NPT088 or PBS. This procedure, which has been successfully used in other published studies of anti-amyloid monoclonal antibodies containing Fc-Hu-IgG_1 like NPT088 [18], has been shown to deplete CD4+ T-cells resulting in tolerance of foreign antigens [19]. To minimize variability in pathology and disease progression, all analyses reported were conducted on male mice. All procedures were performed in accordance with local and federal guidelines for the ethical use and treatment of animals and under the supervision of an institutional animal care and use committee.

2.4. Behavioral testing

2.4.1. Spontaneous alternation

Mice were placed into one arm of a Y-maze (Arms: 30 cm L × 10 cm W × 20 cm H) facing the central zone, and activity was monitored for a period of 10 minutes. Light levels in the Y-maze were approximately 210 lux. Between subjects, the arenas were wiped with 70% ethanol (EtOH) followed by distilled water (dH_2O) to reduce olfactory cues. A successful alternation occurred when a mouse entered a different arm on three consecutive arm entries. Locomotor activity and arm entries were quantified by with TopScan (CleverSys, Reston, VA). Arm entry occurred when a subject's center of mass crossed into the beginning of an arm. Alternation rate was calculated as: $number\ of\ alternations/number\ of\ arm\ entries - 2$. Statistical analysis was performed with 1-way ANOVA and post-hoc comparisons made with Dunnett test. P value was set at $\leq .05$.

2.4.2. Novel object recognition

NOR was performed in an open field arena (50 cm L × 50 cm W × 40 cm H; ~210 lux). Between subjects, the arenas were wiped with 70% EtOH followed by dH_2O. Testing was conducted over 2 days. Day 1 was a 30-minute arena habituation session where individual mice were permitted to freely explore the empty arena. Day 2 included both the sample and test phase of NOR. During the sample phase, mice were placed into the arena and permitted to freely explore two identical objects for 15 minutes. Four hours after completion of the sample phase, mice were placed back into the arena and permitted to freely explore a familiar and a novel object for 10 minutes. For each phase of the task, mice were placed in the center of the arena at the beginning of a session, and the arena and objects were thoroughly cleaned with 70% EtOH then dH_2O at the end of each session. Objects were placed 5 cm away from the walls of the arena, and location of objects in the sample and test phases was identical. All objects were screened in a separate cohort of mice for differences in exploratory behavior elicited from mice, and only objects that elicited comparable levels of exploratory behavior when both were novel were used in this study. Objects (bowl & jar, approx. 5 cm in each dimension) were counterbalanced across all groups to further minimize any potential effect of object on this task. Locomotor activity and object explorations were quantified with TopScan (CleverSys). An object exploration occurred when the subject's nose was within 2 cm of the object, and the midpoint of the subject's body was

beyond 2 cm from the object. NOR was assessed using the discrimination index ($[T_{novel} - T_{familiar}]/T_{total}$). Statistical analysis was performed either with 1-way ANOVA and post-hoc comparisons performed with Dunnett test when there were three or more treatment groups, or a *t* test when only 2 treatment groups were compared. *P* value was set at $\leq$.05.

2.4.3. Limb clasping

Mice were raised by the tail for 5 seconds over the home cage and scored for limb clasping on a scale of 0–5. Zero = no limbs clasping, 1 = one limb clasping, 2 = two limbs clasping, 3 = three limbs clasping, 4 = all four limbs clasping, 5 = all limbs clasping severely. Scores from two independent observers simultaneously observing the mice were averaged. Statistical analysis was performed with 1-way ANOVA and post-hoc comparisons made using Dunnett test. *P* value was set at $\leq$.05.

2.5. Tissue collection

Mice were deeply anesthetized with a combination of dexdomitor (0.3 mg/kg) and telazol (20 mg/kg), transcardially perfused with saline and brains were removed. In some experiments (Section 3.3.3), brains were weighed on a digital scale immediately after removal from the skull. Brains were hemisected, and the right hemibrain was immersion fixed in 4% paraformaldehyde (in PBS, pH 7.4) for 2 days at 4°C. After fixation, brains were transferred to a 30% sucrose solution (in PBS, pH 7.4) and cut in the coronal or sagittal plane at 40 μm on a freezing sliding microtome. The left hemisphere was immediately microdissected on wet ice, and frontal brain, caudal brain, hippocampus, cerebellum, and olfactory bulb were frozen in separate tubes in liquid nitrogen.

2.6. CSF collection

In some mice, cerebrospinal fluid (CSF) was collected before obtaining brain tissue. After administration of anesthesia (see Section 2.5), each mouse was positioned such that CSF flowed backward. A small incision in the skin and muscles permitted puncture of the cisterna magna membrane with the tip of a 30G needle. A gel-loading pipette tip covered the puncture hole to create a seal and suction was applied to draw CSF (6–12 μL). CSF was centrifuged at 5000× g for 10 minutes at 4°C and the resulting supernatant aliquoted for analysis of $A\beta_{1-xx}$ (see Section 2.9).

2.7. Immunoprecipitation of Aβ by NPT088 in brain tissue

2.7.1. Tissue homogenization and fractionation

Frozen cortices from aged Tg2576 mice (20 mo) were homogenized and processed [20]. After a tris-buffered saline (TBS) and Triton-X extraction, insoluble Aβ was collected by extraction with 70% formic acid (FA) followed by sonication with a bath sonicator. FA extraction was restricted to 3 hours to ensure that samples contained substantial amounts of higher molecular weight aggregates. After centrifugation (175,000× g for 30 minutes at 4°C), the supernatant was collected and frozen at −80°C. Before use, the FA fraction was neutralized with 1M Tris base (1:27 v:v). The FA-soluble fraction used in the immunoprecipitation experiments is referred to as the "Insoluble" fraction.

2.7.2. Immunoprecipitation

The insoluble fraction was incubated with protein A/G sepharose beads (GE Healthcare, cat # 17-0618-01; 17-0780-01) for 60 minutes at 4°C. After centrifugation (3500× g for 2 minutes at 4°C), the supernatant was collected and diluted 1:1 in PBS buffer with 20% Superblock (ThermoFisher, cat # 37,515) and 0.1% Tween. NPT088-coupled Dynabeads (Invitrogen, cat # 2017-08) were incubated with the insoluble fraction for 1.5 hours at 37°C. Beads were washed in 300-mM NaCl phosphate buffer with 0.05% Tween followed by washes in 137-mM NaCl phosphate buffer +0.05% Tween. Beads were incubated in 1 × lithium dodecyl sulfate reducing sample buffer (LDS, ThermoFisher, cat# NP0007) for 10 minutes at 95°C, and bound proteins were separated on NuPAGE 4%–12% Bis-Tris gels (Life Technologies, cat: WG1401BX10). After transfer to nitrocellulose membrane, the membrane was boiled in PBS for 2 min and blocked in 5% milk in TBS–0.05% Tween for 1 hour at room temperature (RT). Aβ was detected with 6E10 (Covance, cat#: 39,320), which recognizes both APP and Aβ [see 21], in 5% milk in TBS–0.05% Tween for 18 hours at 4°C.

2.8. Quantification of $A\beta_{42}$ in brain tissue

2.8.1. Tissue homogenization and fractionation

Frozen frontal brain (rostral from Bregma) and hippocampus was homogenized and processed as previously described [22]. Briefly, tissue was thawed on ice, weighed, and homogenized at a concentration of 1 mL/150 mg, with buffer consisting of 10-mL RIPA (Sigma, cat #R0278), 1 Complete ULTA tablet (Roche 05-892-970-001), 1 phosSTOP tablet (Roche 04-906-845), and 0.5-mL 5M EDTA. Brains were sonicated on ice (Fisher Scientific model FB705 ultra tip sonicator, 10 seconds) and spun at 100,000× g for 30 minutes at 4°C. The supernatant (S1) was collected, aliquoted, and frozen at −80°C until further use. The remaining pellet was homogenized in 70% formic acid (FA) to a concentration of 2 μL/mg tissue. The pellet was sonicated on ice, as above, and spun at 100,000× g for 30 minutes at 4°C. The supernatant (S2) was collected, aliquoted, and frozen at −80°C. Just before use, S2 was neutralized with 1M Tris base (1:20 v:v). In this study, S1 is referred to as the "Soluble" fraction and S2 as the "insoluble" fraction.

2.8.2. $A\beta_{42}$ ELISA

Levels of Aβ1–42 ($A\beta_{42}$) were measured using the Innotest β-amyloid$_{(1–42)}$ test kit (FujiRebio, Malvern, PA, cat #: 80,177, lot #: 232810). The investigator performing the analysis was blind to treatment groups. Samples were run according to kit instructions. After adjustment for log-transformation and dilution, the unknown values were normalized to protein concentration, obtained from the same sample aliquot using a BCA assay (ThermoFisher, Carlsbad, CA, cat # 23,252), to derive final $A\beta_{42}$ values in pmol/g. Values were excluded if they were either below the lower limit of quantification (LLOQ; <0.04 pmol/g and 0.09 pmol/g, for soluble and insoluble fractions, respectively) or if agreement among dilution values was <70%. Statistical analysis was performed with 1-way ANOVA and post hoc comparisons made with Dunnett test. *P* value was set at ≤.05.

2.9. Quantification of $A\beta_{1–38}$, $A\beta_{1–40}$, and $A\beta_{1–42}$ in CSF

CSF levels of total human $A\beta_{1–42}$, $A\beta_{1–40}$, and $A\beta_{1–38}$ were measured using MesoScale Discovery Aβ Peptide Panel 1 (6E10) VPLEX kit (cat #K15200E). Samples were run according to manufacturer's instructions. Unknown values are reported as pg Aβ/mL CSF. Statistical analysis was performed with 1-way ANOVA, and post hoc comparisons were made with Dunnett test. *P* value was set at ≤.05.

2.10. Neuropathology

2.10.1. Tissue sectioning and processing

Right hemibrains were sectioned coronally at 40 μm, or sagittally at 30 μm, on a freezing sliding microtome and stored in a glycerol-based cryoprotectant at −20°C before immunostaining of $A\beta_{1–x}$ (82E1) and p-tau (AT8). Sectioning and staining were performed either at NeuroScience Associates (NSA, Knoxville, TN) using their MultiBrain Technology and in-house staining procedures (https://www.neuroscienceassociates.com/technologies/multibrain/) or in the laboratory of E. Mufson at Rush University Medical Center (Chicago, IL).

In the Mufson laboratory, immunostaining was performed at RT on floating sections that were incubated overnight in primary antibodies (biotinylated 82E1, IBL cat # 10,326, 1:2000; AT8, ThermoFisher cat # MN1020, 1:3000; biotinylated AT8, ThermoFisher cat # MN1020B, 1:3000). For non-biotinylated primary antibodies, sections were incubated in biotinylated secondary antibodies directed against the appropriate species IgG. Detection of biotinylated reagents was performed with the Vectastain Elite ABC Kit (Vector Laboratories cat #: PK-6100) for 60 minutes and the DAB Peroxidase Substrate Kit (Vector Laboratories cat #: SK-4100) according to the manufacturer's instructions.

Fibrillary Aβ was visualized using thioflavin S (thioS) histochemistry, and cytoarchitectonics were visualized with thionine staining performed by NSA.

2.10.2. Imaging and analysis

Neuropathologic analyses of all immunohistochemical labeling were performed on 12-bit monochrome images of the dorsal hippocampus or overlying cortex in 2–3 sections/brain at 240 μm (coronal) or 180 μm (sagittal) intervals. The lowest magnification at which measurements were not significantly different from higher magnifications was chosen for image capture. Magnification was selected based on measurements in the same area in a section at different magnifications in five mice. Sections were at comparable rostro-caudal or medial-lateral levels between brains, and all images were captured at the same exposure time. MetaMorph software was used for image analyses. Total area of 82E1 immunostaining (very diffuse Aβ excluded) within the regions of interest (ROIs; entire dorsal hippocampus area and overlying cortical area) and AT8 immunostaining in the entire dorsal hippocampus area was quantified in thresholded images (magnification of 4×) and expressed as a percentage of the ROI area. Quantification of the fluorescent signal of thioS was performed similarly in Tg2576 mice, and the number of thioS-positive plaques was also counted. ThioS in sagittal images (magnification of 10×) of the cortex of rTg2576 mice was quantified as a percentage of a ROI approximately 0.19 mm^2, one designed to fit within all the variations in brain size seen in this model for tau pathology. The thickness of the CA1 pyramidal cell layer was measured at four evenly spaced points in the region between the CA1/CA2 boundary and the apex of CA1 in each section using ImageJ software and these four values were averaged for each brain. Data were analyzed with a 1-way ANOVA and post hoc comparisons made with Dunnett test. *P* value was set at ≤.05.

3. Results

3.1. Characterization of NPT088 in vitro

NPT088 is a novel immunoglobulin fusion protein that is bivalent for GAIM (Fig. 1A). We previously demonstrated in vitro that both M13 and NPT088 efficiently bind to Aβ fibers, and that neither M13 nor NPT088 exhibit binding to Aβ monomers [14]. Although fibrillar species of Aβ are prevalent in plaques, cognitive impairment [23,24] and disruption of synaptic plasticity [24,25] are associated with lower molecular weight toxic oligomers of Aβ. To determine whether NPT088 could inhibit cytotoxicity induced by Aβ oligomers, we investigated whether pretreatment of $A\beta_{42}$ ADDLs with NPT088-inhibited cytotoxicity induced in differentiated N2a cells. Exposure of differentiated N2a cells to ADDLs (2 μM, 9 μg/mL) for 24-hour–induced robust cytotoxicity (Fig. 1B). Pretreatment of ADDLs with NPT088 for 3 hours significantly inhibited

cytotoxicity (Fig. 1B, Dunnett's post-hoc: 46 nM vs. ADDL, $P < .0001$; 4.6 nM vs. ADDL, $P < .0001$, 0.46 nM vs. ADDL, $P = .0009$). When ADDLs and NPT088 were added to cultures simultaneously, no effect was observed on cytotoxicity (Fig. 1B, Dunnett's post-hoc: 0.46 nM [Time 0] vs. ADDL, $P = .4$) indicating that effect of NPT088 on cytotoxicity was due to binding to ADDLs and not a nonspecific interaction with N2a cells. Moreover, the IC_{50} values of NPT088 calculated in these assays are 5–50 nM, suggesting that NPT088 binds Aβ and neutralizes toxicity at substoichiometric ratios (1 NPT088: 40-400 $A\beta_{42}$ monomers), consistent with the hypothesis that the NPT088-mediated inhibition of cytotoxicity was due to interaction with oligomeric species of Aβ.

To further demonstrate NPT088 binding to Aβ, a formic acid–soluble (FA) fraction of Tg2576 brain lysates was used to assess the ability of NPT088 to immunoprecipitate Aβ. The Aβ in the FA fraction is a heterogeneous mix of monomeric Aβ and non-denatured larger amyloid aggregates (Supplementary Fig. 1). NPT088 successfully immunoprecipitated various species of Aβ from the FA fraction of Tg2576 brain lysates (Fig. 1C). Although the conformation of NPT088-interacting species in the FA fraction is not known, NPT088 does not bind to Aβ monomers in vitro and likely interacts with aggregated Aβ species consisting of SDS-stable Aβ dimers and higher order Aβ-mers (Fig. 1C). The hAPP observed in these lysates is associated with high molecular weight, aggregated Aβ (Supplementary Fig. 1) and is consistent with previous studies demonstrating inclusion of misfolded hAPP in growing intracellular amyloid aggregates [26]. To test for effects of NPT088 on amyloid fibers, $A\beta_{42}$ fibers were incubated with NPT088 (0.25 μM) for 7 days, and this resulted in remodeling of fibrillar Aβ into amorphous deposits (Fig. 1D, see also Supplementary Fig. 2A and 2B). In addition, NPT088 remodels fibers assembled from the microtubule binding region of tau (Supplementary Fig. 2C), which is notable as these fibers are transmission-competent after sonication (Supplementary Fig. 3). All the remodeling data presented in the present study are consistent with previous remodeling assays of GAIM-based molecules [14]. Collectively, the in vitro characterization of NPT088 indicates that it effectively targets several species of aggregated Aβ, suggesting that it could mediate reduction of Aβ pathology in vivo.

3.2. NPT088 in Tg2576 mice

3.2.1. Brain exposure of NPT088

To confirm that NPT088 was able to enter the central nervous system (CNS) when administered via IP injection, NPT088 was quantified in homogenates of frontal cortex from aged (19–20 mo) male Tg2576 mice after a single, IP injection (10 mg/kg). Levels of NPT088 were maximal 1 day after injection (4.7 ng/mg; Supplementary Fig. 4). NPT088 was still detectable 14 days after injection (Supplementary Fig. 4). These results confirm that NPT088 is able to enter the CNS of aged Tg2576 mice after IP injection.

3.2.2. Improvement in cognitive function

NPT088 was engineered to contain an IgG_1-Fc (Fig. 1A), which provides antibody-like pharmacokinetic, tissue distribution, and effector function properties. To assess whether systemically administered NPT088 affected the cognitive function, performance in the spontaneous alternation and NOR tasks was measured. Previous studies have shown that aged Tg2576 mice exhibit significant deficits in spontaneous alternation and NOR [16,27,28]. After administration of 10 doses of NPT088 to Tg2576 mice (16–19 months at the beginning of the experiment, 18–21 months at time of testing), spontaneous alternation in the Y-maze was measured during week 10 (Fig. 2A). A significant increase in the spontaneous alternation rate was observed in the highest dose (20 mg/kg) group (Dunnett's post-hoc, 20 mg/kg vs. PBS, $P < .05$). After administration of a further four doses of NPT088, NOR was assessed during week 14 (19–22 months at time of testing; Fig. 2B). Similar to spontaneous alternation in the Y-maze, a significant increase in novel object recognition was observed at the highest (20 mg/kg) dose (Dunnett's post-hoc, 20 mg/kg vs. PBS, $P < .05$).

3.2.3. Reduction of soluble & insoluble Aβ42

The improvements in cognitive performance were accompanied by a significant reduction of soluble and insoluble $A\beta_{42}$ in both the hippocampus (Soluble: Fig. 2C, Dunnett's post-hoc, 0.2 mg/kg vs. PBS, $P < .01$; 2 mg/kg vs. PBS, $P < .01$; 20 mg/kg vs. PBS, $P < .05$; Insoluble: Fig. 2D, Dunnett's post-hoc, 2 mg/kg vs. PBS, $P < .05$) and frontal cortex (Soluble: Fig. 2E, Dunnett's post-hoc, 0.2 mg/kg vs. PBS, $P < .01$; 2 mg/kg vs. PBS, $P < .01$; 20 mg/kg vs. PBS, $P < .05$; Insoluble: Fig. 2F, Dunnett's post-hoc, 2 mg/kg vs. PBS, $P < .01$; 20 mg/kg vs. PBS, $P < .05$). Reductions in soluble and insoluble species of $A\beta_{42}$ are consistent with the ability of NPT088 to interact with both soluble (Fig. 1B and 1C) and insoluble fibrillar species of Aβ (Fig. 1D, Supplementary Fig. 2A and 2B). These results indicate that NPT088, when administered systemically, was able to mitigate cognitive impairments in aged Tg2576 mice, potentially through removal of soluble and insoluble species of $A\beta_{42}$.

3.2.4. Reduction of Aβ neuropathology

To confirm NPT088 can engage Aβ and mediate its clearance from the brain, tissue sections from the paraformaldehyde-fixed hemisphere of aged Tg2576 mice were immunostained for Aβ. Mice treated with NPT088 demonstrated significantly less Aβ immunostaining in the hippocampus relative to mice treated with PBS (Fig. 3A and 3B; Fisher post hoc, 0.2 mg/kg vs. PBS, $P < .05$; 2 mg/kg vs. PBS, $P < .05$; 20 mg/kg vs. PBS, $P < .05$).

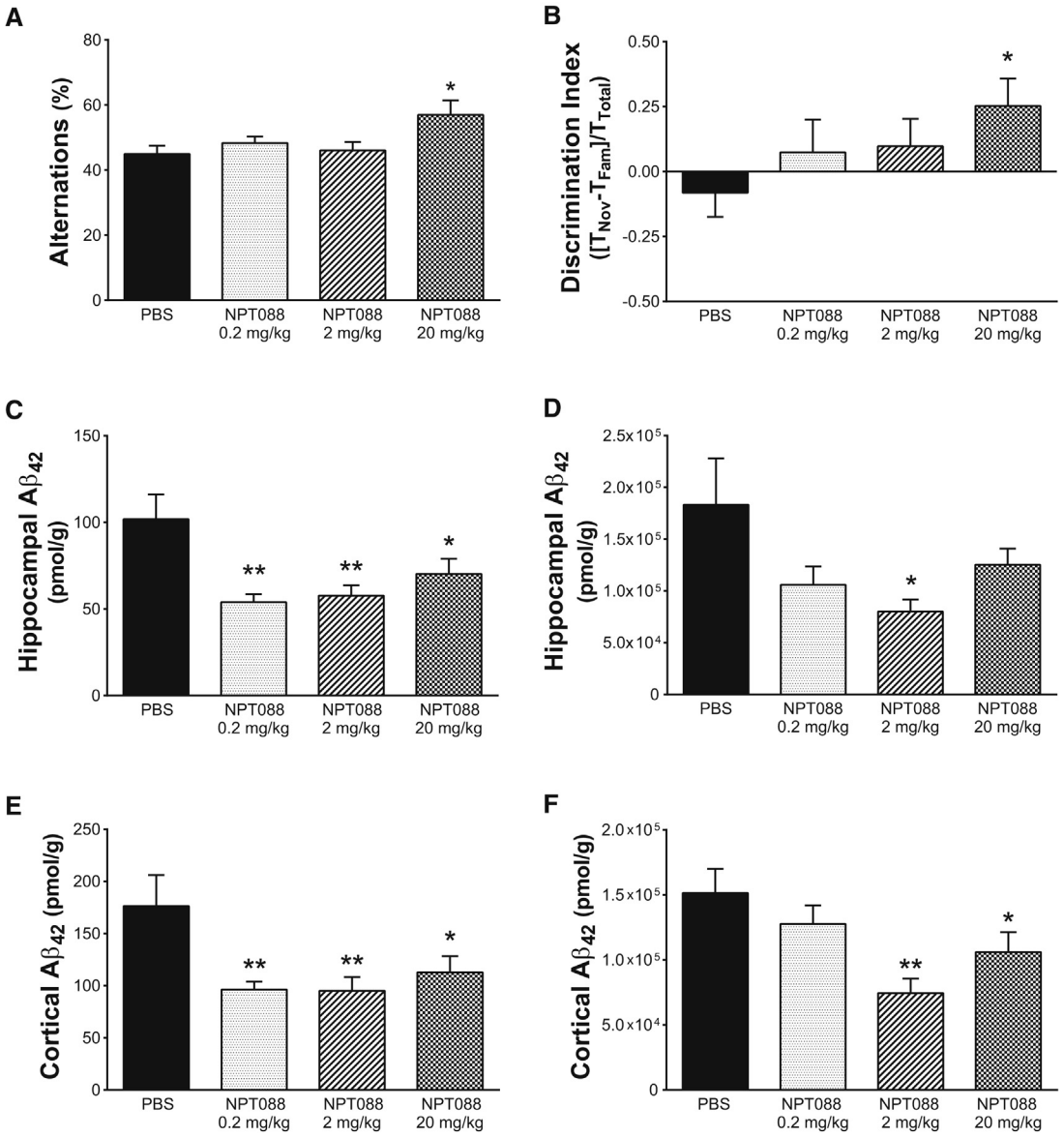

Fig. 2. Systemically administered NPT088 improves cognition in aged Tg2576 mice. Behavior was assessed in aged Tg2576 mice (16–19 months at the start of dosing) after repeated, weekly IP administration of NPT088. (A) Spontaneous alternation in a Y-maze was significantly increased after 10 weeks of weekly dosing with NPT088 at 20 mg/kg ($q_{47} = 2.8$, $P = .01$). N = 13 (PBS), 13 (0.2 mg/kg), 12 (2 mg/kg), 13 (20 mg/kg). (B) Performance of novel object recognition was significantly increased after 14 weeks of weekly dosing with NPT088 at 20 mg/kg ($q_{40} = 2.1$, $P = .05$). N = 11 (PBS), 11 (0.2 mg/kg), 12 (2 mg/kg), 10 (20 mg/kg). (C) Systemic NPT088 significantly reduced levels of $A\beta_{42}$ from the soluble fraction of hippocampus at all doses tested (0.2 mg/kg: $q_{44} = 3.6$, $P = .003$; 2 mg/kg: $q_{44} = 3.3$, $P = .005$; 20 mg/kg: $q_{44} = 2.4$, $P = .05$). N = 12 (PBS), 11 (0.2 mg/kg), 12 (2 mg/kg), 13 (20 mg/kg). (D) Systemic NPT088 significantly reduced levels of $A\beta_{42}$ from the insoluble fraction of hippocampus when administered at 2 mg/kg ($q_{46} = 2.7$, $P = .02$). N = 13 (PBS), 12 (0.2 mg/kg), 12 (2 mg/kg), 13 (20 mg/kg). (E) Systemic NPT088 significantly reduced levels of $A\beta_{42}$ from the soluble fraction of cortex at all doses tested (0.2 mg/kg: $q_{47} = 3.1$, $P = .01$; 2 mg/kg: $q_{47} = 3.1$, $P = .01$; 20 mg/kg: $q_{47} = 2.4$, $P = .05$). N = 13 (PBS), 13 (0.2 mg/kg), 13 (2 mg/kg), 12 (20 mg/kg). (F) Systemic NPT088 significantly reduced levels of $A\beta_{42}$ in the insoluble fraction of cortex at 2 and 20 mg/kg (2 mg/kg: $q_{47} = 3.6$, $P = .002$; 20 mg/kg: $q_{47} = 2.1$, $P = .05$). N = 13 (PBS), 12 (0.2 mg/kg), 13 (2 mg/kg), 13 (20 mg/kg). In all panels, asterisks indicate significant difference versus Tg-PBS.

Similar to observations made in the hippocampus, significant reductions of cortical Aβ immunostaining were observed in all treatment groups (Fig. 3C and 3D; Fisher post hoc, 0.2 mg/kg vs. PBS, $P < .01$; 2 mg/kg vs. PBS, $P < .001$; 20 mg/kg vs. PBS, $P < .05$). Analysis of cortical thioS histochemical staining revealed significant decreases in the number of thioS-reactive plaques only in the 2 and 20 mg/kg but not the 0.2 mg/kg treatment groups (Fig. 3E and 3F; Fisher's post hoc, 2 mg/kg vs. PBS, $P < .05$; 20 mg/kg vs. PBS, $P < .05$). Reduction of Aβ plaque was not associated with an increase in microhemorrhage (Supplementary Fig. 5) as detected using Perls iron staining.

3.2.5. *Reduction in levels of Aβ1-xx in CSF*

To determine whether NPT088 facilitated movement of Aβ from parenchyma into adjacent fluid compartments,

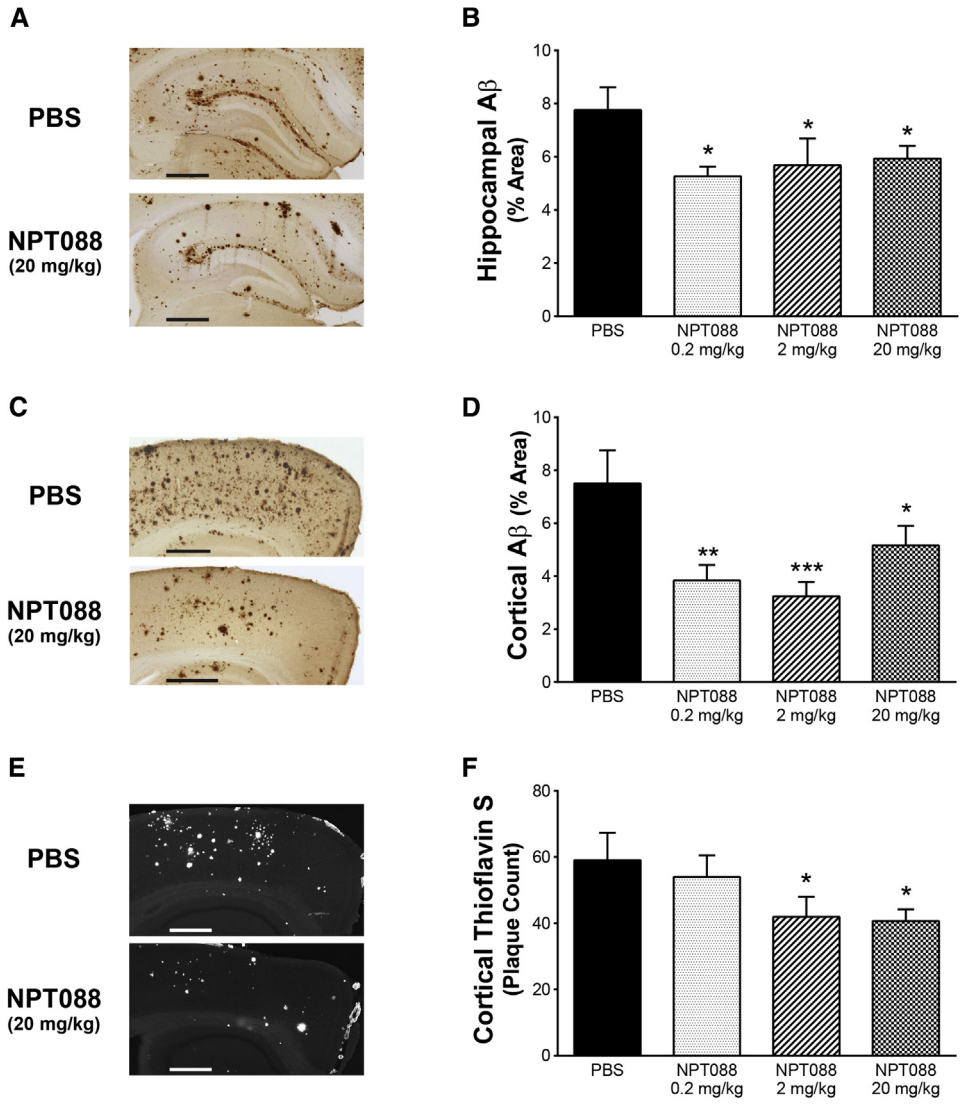

Fig. 3. Systemically administered NPT088 reduces Aβ plaque and Aβ42 in aged Tg2576 mice. Aged Tg2576 mice (16–19 months at the start of dosing) received 14 weeks of weekly, IP injections of NPT088 at ascending doses (0.2, 2, 20 mg/kg). Tissue was harvested 24 hours after the last injection. (A) Representative images of 82E1-immunostained Aβ in the hippocampus showing reduction after treatment with NPT088. Scale bars = 500 μm. (B) Summary quantification of 82E1 immunostaining from three coronal sections at 240-μm intervals indicating significant reduction of total Aβ plaque in the hippocampus at all doses tested. N = 11 (PBS), 10 (0.2 mg/kg), 12 (2 mg/kg), 10 (20 mg/kg). Asterisks indicate significant difference versus Tg-PBS. (C) Representative images of 82E1 immunostaining in the cortex showing reduction of Aβ after treatment with NPT088. Scale bars = 500 μm. (D) Summary quantification of 82E1 immunostaining from three sections indicating significant reduction of Aβ in the hippocampus at all doses tested. N = 11 (PBS), 10 (0.2 mg/kg), 11 (2 mg/kg), 9 (20 mg/kg). Asterisks indicate significant difference vs. Tg-PBS. (E) Representative images of thioflavin-S staining in the cortex showing reduction in the number of fibrillar Aβ plaques after treatment with NPT088. Scale bars = 500 μm. (F) Summary quantification from two sections of thioflavin-S staining indicating significant reduction of fibrillar Aβ plaque number in the hippocampus at 2 and 20 mg/kg (2 mg/kg: $t_{41} = 1.9$, $P = .04$; 20 mg/kg: $t_{41} = 2.0$, $P = .03$). N = 10 (PBS), 11 (0.2 mg/kg), 13 (2 mg/kg), 11 (20 mg/kg). Asterisks indicate significant difference versus Tg-PBS.

CSF was collected from aged Tg2576 mice (20–21 months at study start) after 13 weeks of weekly IP dosing with NPT088. CSF was also collected from a separate group of mice before initiation of dosing to gain insight into baseline levels of Aβ. Weekly dosing with NPT088 was associated with significantly less $Aβ_{1–38}$ (Fig. 4A; Dunnett's post hoc, Tg-NPT088 vs. Tg-PBS, $P < .05$) and $Aβ_{1–40}$ (Fig. 4B; Dunnett's post hoc, Tg-NPT088 vs. Tg-PBS, $P < .05$) compared to PBS-treated Tg2576 mice. Dosing with NPT088 did not significantly affect CSF levels of $Aβ_{1–42}$ (Fig. 4C; Dunnett's post hoc, Tg-NPT088 vs. Tg-PBS, $P = .15$). Levels of $Aβ_{1–40}$ and $Aβ_{1–42}$ observed here were consistent with previously published observations in aged Tg2576 mice [29]. Collectively, these results indicate that NPT088 does not shunt soluble species of Aβ into nonparenchymal fluidic compartments suggesting that NPT088-mediated reductions in Aβ occur by direct remodeling of insoluble species

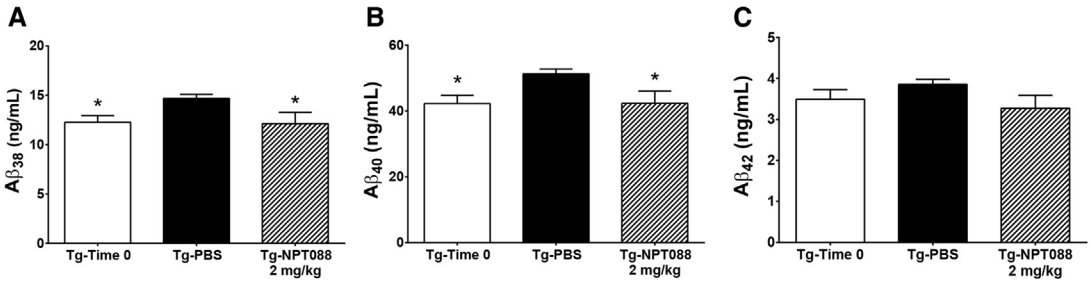

Fig. 4. Systemically administered NPT088 reduces Aβ in CSF of aged Tg2576 mice. CSF was collected from aged Tg2576 mice (20–21 months at experiment start) before dosing or after administration of 13 weeks of weekly, IP injections of NPT088 (2 mg/kg). (A) The concentration of $A\beta_{1-38}$ significantly increased in CSF from aged Tg2576 mice over 13 weeks ($q_{54} = 2.3$, $P = .05$). Weekly IP dosing with NPT088 significantly reduced $A\beta_{1-38}$ in CSF ($q_{54} = 2.4$, $P = .04$). N = 19 (Tg-Time 0), N = 21 (Tg-PBS), N = 17 (Tg-NPT088). (B) The concentration of $A\beta_{1-40}$ significantly increased in CSF from aged Tg2576 mice over 13 weeks ($q_{53} = 2.5$, $P = .03$). Weekly IP dosing with NPT088 significantly reduced $A\beta_{1-40}$ in CSF ($q_{53} = 2.4$, $P = .04$). N = 19 (Tg-Time 0), 20 (Tg-PBS), N = 17 (Tg-NPT088). One significant outlier (Grubb test) in the Tg-PBS group (77.7 ng/mL) was excluded from $A\beta_{1-40}$ analysis. (C) The concentration of $A\beta_{1-42}$ did not significantly change in CSF from aged Tg2576 mice over 13 weeks of dosing ($q_{52} = 1.1$, $P = .4$). Weekly IP dosing with NPT088 did not affect $A\beta_{1-42}$ in CSF ($q_{52} = 1.8$, $P = .15$). N = 19 (Tg-Time 0), 20 (Tg-PBS), N = 17 (Tg-NPT088). One significant outlier (Grubb test) in the Tg-PBS group (6.2 ng/mL) was excluded from $A\beta_{1-42}$ analysis. Asterisks indicate significant difference versus Tg-PBS.

and/or clearance of soluble and/or insoluble species via cellular mechanisms (i.e., phagocytosis).

3.3. NPT088 in rTg4510 mice

3.3.1. Improvement in cognitive and motor function

A unique feature of NPT088 is its ability to bind to and remodel amyloid aggregates independent of primary sequence, including aggregates of tau [14]. To determine whether NPT088 was able to affect tau neuropathology in vivo, we dosed the rTg4510 tauopathy mouse model [17] with NPT088 (20 mg/kg) or PBS weekly (IP) for 14 weeks (3.5 months at beginning of experiment). Previous studies indicate that rTg4510 mice exhibit significant deficits in the novel object recognition [30]. Performance of PBS-treated rTg4510 mice (6.3 months at the time of testing) in the NOR task tended to be lower than WT littermate mice (Fig. 5A; Fisher post hoc, WT vs. Tg-PBS, $P < .1$). After 14 weeks of NPT088 treatment, a significant improvement in performance of the NOR task was observed in rTg4510 mice (Fig. 5A; Fisher post hoc, Tg-PBS vs. Tg-NPT088, $P < .05$). Importantly, performance in the test was not correlated with spontaneous locomotor behavior (Supplementary Fig. 6), indicating that the changes in cognitive performance were not due to changes in motor behavior.

In addition to cognitive impairments, rTg4510 mice exhibit atrophy of dorsal corticospinal tracts leading to limb clasping and other functional motor deficits [31,32]. Such a clasping phenotype has been observed in several tau transgenic mouse models at young ages including P301S mice at age of 3 months [33], line 44 mice at age of 5 months [34], and Tau-4R/2N mice at age of 6–8 weeks [35]. To determine whether NPT088 altered functional motor performance of rTg4510 mice, we assessed limb clasping at the age of 5–6 months after 14 weeks of weekly dosing with NPT088. As expected, PBS-treated rTg4510 mice exhibited significantly more limb clasping when suspended by the tail relative to WT littermates (Fig. 5B; Dunnett's post hoc, $P < .05$). Treatment with NPT088 significantly ameliorated limb clasping abnormalities in rTg4510 mice (Fig. 5B; Dunnett's post hoc, $P < .05$).

3.3.2. Reduction in p-tau and fibrillar tau

To determine whether treatment with NPT088 was able to reduce levels of p-tau immunostaining and fibrillar tau species in brain regions relevant to cognition, AT8 (pSer202/pThr205) p-tau and thioS staining were quantified. A significant decrease in AT8 p-tau immunostaining of the somatodendritic compartment in hippocampal pyramidal cells was observed after NPT088 treatment (Fig. 5C; Mann–Whitney test, $P < .05$). Moreover, significant decreases in thioS staining of cortical neurons were observed in tissue from mice treated with NPT088 compared to PBS-treated mice (Fig. 5D; Mann–Whitney test, $P < .05$). Additionally, frozen cortex from the contralateral hemisphere was analyzed biochemically via Western blot using AT8, pSer422, and AT270 antibodies. Significant reductions of AT8 were observed in a high-salt insoluble-pellet enriched for neurofibrillary tangles (Supplementary Fig. 7A; *t* test, $P < .05$). In a Triton-X soluble fraction, levels of pSer422 were significantly reduced (Supplementary Fig. 7B; *t* test, $P < .05$), and a trend was observed for reduction of AT270 (Supplementary Fig. 7C; *t* test, $P < .08$). The reductions in levels of AT8, pSer422, and AT270 were replicated in a separate cohort of mice (AT8: Supplementary Fig. 7D; pSer422: Supplementary Fig. 7E; AT270: Supplementary Fig. 7F).

3.3.3. Aged rTg4510: reduction in brain atrophy and fibrillar tau and cognitive improvement

A hallmark of the rTg4510 tauopathy mouse model is severe forebrain neurodegeneration, which is significant in mice aged >5 months [31]. To assess whether NPT088 could affect the amount of neurodegeneration exhibited by this mouse, rTg4510 mice (5.7 months at study start) received 13 weekly IP doses of NPT088 (2 mg/kg). Brains

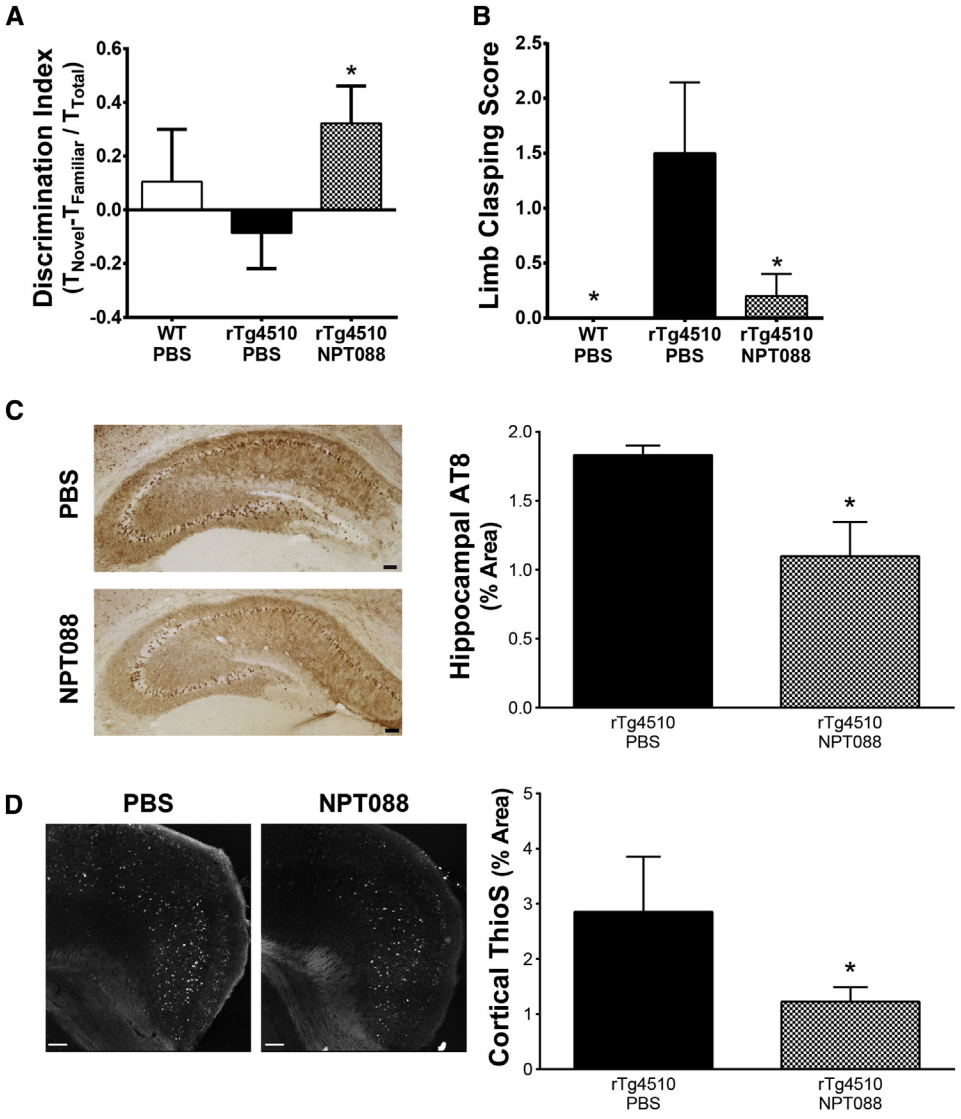

Fig. 5. Systemically administered NPT088 improves cognitive and motor phenotypes and reverses tau pathology in rTg4510 mice. Behavior and levels of p-tau were assessed in rTg4510 mice (3.5 mo) that received 14 weeks of weekly IP treatment with NPT088 (20 mg/kg) or PBS. (A) rTg4510 mice treated with NPT088 exhibited significantly better performance in the novel object recognition task relative to rTg4510 mice receiving PBS ($t = 2.3$, $df = 7$, $P = .02$). N = 4 (WT-PBS), 4 (Tg-PBS), 5 (Tg-NPT088). Asterisk indicates significant difference versus rTg4510-PBS. (B) rTg4510 mice exhibited significant limb clasping relative to WT mice when suspended by the tail ($q_9 = 2.8$, $P = .02$). Treatment with NPT088 significantly reversed limb splay abnormality ($q_9 = 2.8$, $P = .02$). N = 4 (WT-PBS), 4 (Tg-PBS), 5 (Tg-NPT088). (C) Treatment with NPT088 significantly decreased somatodendritic AT8 (pSer202/pThr205) immunostaining of aggregated p-tau in pyramidal cells of the hippocampus ($U_{5,5} = 3$, $P = .03$). Representative images of AT8 immunostaining shown to the left of summary quantification. AT8 immunostaining was quantified in three sections at 240-μm intervals per animal. Scale bars = 100 μm. N = 5 (Tg-PBS), 5 (Tg-NPT088). (D) Treatment with NPT088 significantly decreased levels of neuronal thioS in cortex from mice treated with NPT088 ($U_{3,5} = 0$, $P = .02$). Representative images of thioS staining shown to the left of summary quantification. ThioS levels were quantified from three sections per animal. Scale bars = 100 μm. N = 3 (Tg-PBS), 5 (Tg-NPT088). In all panels, asterisk indicates significant difference from Tg-PBS.

from rTg4510 mice receiving NPT088 (8.8 months at study end) weighed significantly more than brains from mice that received vehicle (Fig. 6A and 6B; *t* Test, NPT088 vs. PBS, $P < .05$). The original characterization of rTg4510 mice indicated that neurodegeneration was especially robust in the hippocampus [31]. Thionine-stained sections of hippocampus from rTg4510 mice revealed dramatic atrophy of the hippocampus in mice dosed with PBS that was almost entirely prevented in mice that received NPT088 (Fig. 6C). Hippocampal weight of rTg4510 mice dosed with NPT088 was significantly greater than PBS-treated rTg4510 mice and nearly equivalent to hippocampus weights from rTg4510 mice at the beginning of the study (Fig. 6D; Dunnett's post-hoc, Tg-NPT088 vs. Tg-PBS, $P < .05$; Tg-Time 0 vs. Tg-PBS, $P < .01$). Thickness of stratum pyramidale in area CA1 from rTg4510 mice dosed with NPT088 was significantly greater than that of PBS-treated rTg4510 mice (Fig. 6E; Dunnett's post hoc, Tg-NPT088 vs. Tg-PBS, $P < .05$). A significant reduction in thioS staining in the cortex was observed (Fig. 6F; Dunnett's post hoc,

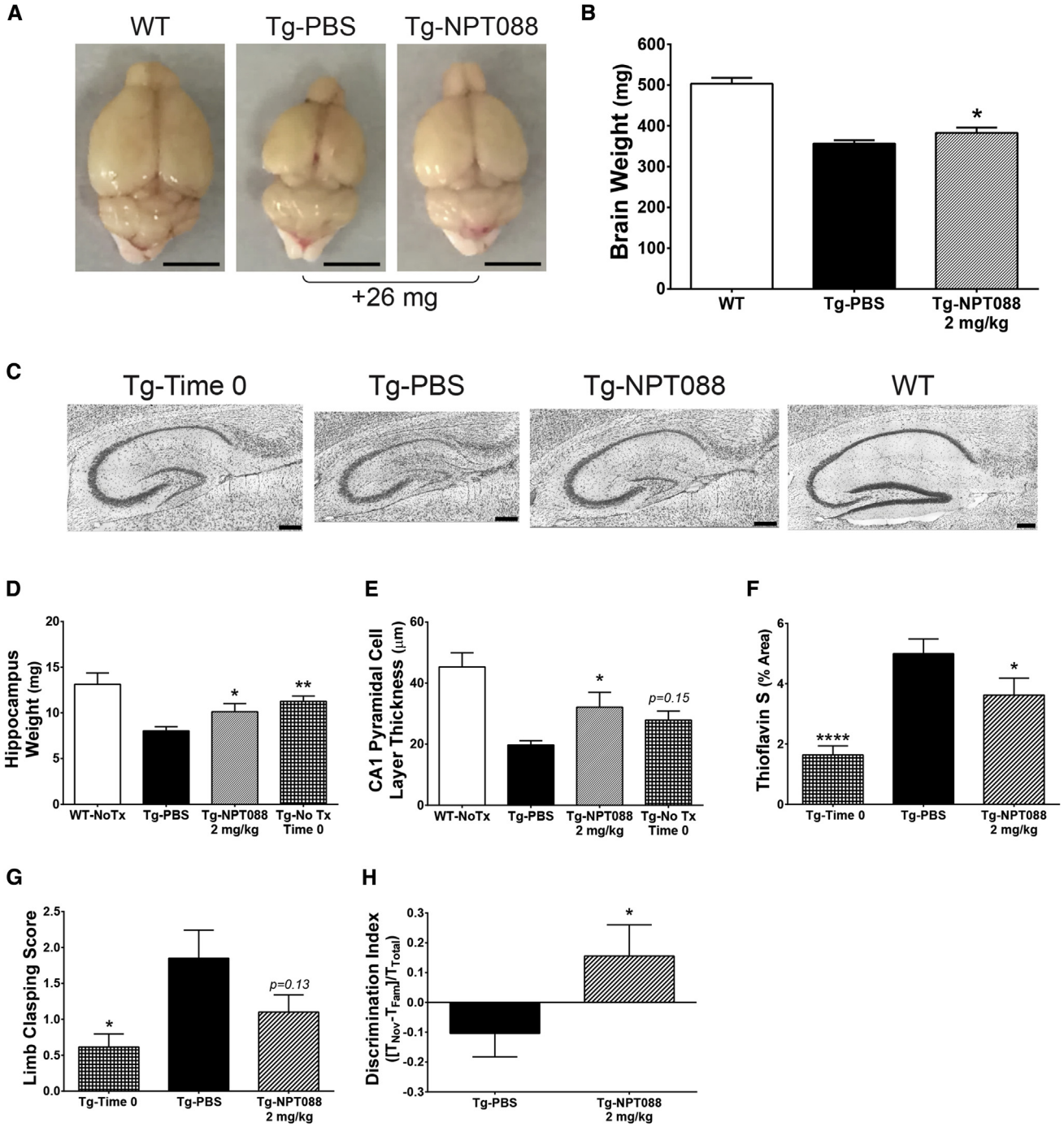

Fig. 6. Systemically administered NPT088 reduced neurodegeneration in rTg4510 mice. rTg4510 mice in this experiment (5.7 mo at start) received 13 weekly IP doses of NPT088 (2 mg/kg) or PBS. Tissue from a group of 13 rTg4510 mice (5.7 mo) was harvested at the beginning of the study to serve as a Time 0 control, and tissue from group of 3 WT mice (8.8 months) was harvested at the end of the study. (A) Representative images of brains from WT mice and rTg4510 mice that received either NPT088 or PBS. Scale bar indicates 5 mm. (B) Wet weight of brains, measured at harvest, from rTg4510 mice receiving NPT088 was significantly more than brain weights measured from rTg4510 mice receiving PBS ($t = 1.7$, $df = 30$, $P = .049$). Brain weights measured from WT mice ($N = 3$) shown for comparative purposes. $N = 3$ (WT), 19 (Tg-PBS), 18 (Tg-NPT088). (C) Representative Nissl-stained sagittal sections of hippocampus from rTg4510 mice harvested at the beginning of the study (Time 0), rTg4510 mice dosed with either PBS (Tg-PBS) or NPT088 (Tg-NPT088), or littermate non-Tg mice (WT). Scale bars are 200 μm. (D) Weight of left hippocampus of rTg4510 mice treated with NPT088 (8.8 mo at harvest) was significantly greater than the weights measured from rTg4510 mice dosed with PBS ($q_{47} = 2.3$, $P = .046$). Hippocampus weight measured from rTg4510 mice harvested at the beginning of the study (5.7 mo) was also significantly greater than weights from rTg4510 mice dosed with PBS ($q_{47} = 3.3$, $P = .004$). Weight of hippocampus from non-Tg littermate mice (WT) is shown for comparison. $N = 3$ (WT), 19 (Tg-PBS), 18 (Tg-NPT088), 13 (Tg-Time 0). (E) Thickness of stratum pyramidale in area CA1 of hippocampus was significantly greater in rTg4510 mice dosed with NPT088 relative to rTg4510 mice that received PBS ($q_{40} = 2.8$, $P = .02$). Stratum pyramidale of area CA1 from tissue harvested at the beginning of the study exhibited a trend for increased thickness relative to mice that were dosed with PBS ($q_{40} = 1.8$,

Tg-NPT088 vs. Tg-PBS, $P < .05$; Tg-Time 0 vs. Tg-PBS, $P < .0001$). Moreover, treatment with NPT088 was associated with functional improvements. After just 4 weeks of dosing (6.7 months at time of test), rTg4510 mice receiving NPT088 exhibited a trend for less severe limb clasping relative to mice dosed with PBS (Fig. 6G; Dunnett's post hoc, Tg-NPT088 vs. Tg-PBS, $P = .13$; Tg-Time 0 vs. Tg-PBS, $P < .05$). Moreover, at the end of the study (8.7 months at time of test), mice treated with NPT088 exhibited significantly better performance in the novel object recognition test (Fig. 6H; t Test, $P < .05$). Collectively, these results are consistent with NPT088 mitigating the neurodegeneration that occurs in rTg4510 mice, which results in subsequent improvements in functional motor and cognitive tests.

4. Discussion

Translation of preclinical therapeutic strategies to successful clinical outcomes is particularly challenging for AD, at least in part because of multiple pathologies and no apparent single-disease mechanism. Most reported therapeutic strategies focused on a single pathologic target such as Aβ [36–38], and the initial wave of Aβ-directed immunotherapies targeted monomeric Aβ with unimpressive efficacy [4–7]. One potential explanation for the failure of such candidates is sequestration of the compound by relatively high concentrations of Aβ monomers from the pathologic oligomeric and fibrillar species, including plaques [10]. In support of this hypothesis, monoclonal antibodies with significant binding to monomeric Aβ produce little or no efficacy when administered to preclinical AD models with pre-existing Aβ deposits [39,40], but efficacy was improved in preclinical models when Aβ production was suppressed with co-administration of a BACE1 inhibitor [41].

NPT088 does not bind monomeric Aβ in vitro [14], binds soluble aggregates of Aβ produced in vitro (Fig. 1B) and derived from Tg2576 mouse brain extracts (Fig. 1C), and prevents cytotoxicity induced by ADDLs (Fig. 1B). In vitro, NPT088 binds and remodels fibrillar forms of Aβ in a concentration dependent manner [14] (Fig. 1D, Supplementary Fig. 2A and 2B). Structural studies of GAIM suggest that the binding domains associate with both templating strands of Aβ fiber required for fiber growth [14]. Surface plasmon resonance binding studies show that a GAIM-fusion is likely to bind a larger surface area (3-to-5-fold more monomers per fiber) [14] as compared to antibodies [42]. The activities of NPT088 on Aβ in vitro translate in vivo to robust reductions of soluble and insoluble forms of Aβ (Fig. 2C–2F), including dense core plaques (Fig. 3A–3D) and fibrillar aggregates (Fig. 3E and 3F) when NPT088 is administered to Tg2576 mice. Although these results do not rule out the possibility that NPT088 binds monomers in vivo, they do suggest that the relative binding affinity of NPT088 on oligomeric and fibrillar Aβ is greater than to monomeric Aβ.

The mechanism of NPT088-mediated lowering of Aβ-associated pathology remains unclear. In vitro, NPT088 appears to remodel Aβ aggregates into amorphous forms (Fig. 1D, Supplementary Fig. 2A and 2B). Therefore, clearance of large brain aggregates (i.e., plaques) could be mediated by the inherent remodeling activity of NPT088, followed by cell-mediated clearance. For example, as described for other Aβ-directed monoclonal antibodies, NPT088, which contains a human-IgG_1-Fc, could engage microglia to facilitate phagocytosis of NPT088-protein aggregate complexes [18]. Although we found no evidence for an increase in the area of microglia staining (Iba1) after 10 or 14 weeks of weekly NPT088 (data not shown), this observation is not inconsistent with other studies on the role of activated microglia in clearance of Aβ, because immunoglobulin Fc-mediated microglia activation is transient after passive immunization [43]. Therefore, we do not rule out Fc-receptor-mediated microglial activation by NPT088 and subsequent phagocytosis as a potential mechanism for NPT088-mediated Aβ clearance. Another potential mechanism for parenchymal clearance of Aβ is via sequestration of Aβ to peripheral fluidic compartments. This mechanism, also known as peripheral sink, is primarily associated with monomer-directed antibodies that facilitate the movement of Aβ from the parenchyma and into CSF and blood [44]. We observed no increases in CSF Aβ levels after NPT088 treatment (Fig. 4). Given the concordance between relative changes in levels of Aβ in CSF and blood [29], especially after treatment with Aβ-directed immunotherapies [45–47], the lack of effect of NPT088 on CSF Aβ levels suggests that NPT088 does not reduce brain Aβ by acting as a peripheral sink or by producing monomer Aβ. Although more characterization of the mechanism of action of NPT088 in vivo is needed, our current preclinical data are consistent with direct remodeling of fibrillar deposits accompanied by microglia uptake of NPT088:Aβ aggregate complexes as a potential clearance mechanism.

$P = .15$). Data from WT mice are shown for comparison. N = 2 (WT), 16 (Tg-PBS), 14 (Tg-NPT088), 13 (Tg-Time 0). One significant outlier (Grubb's test) was excluded from analyses (Tg-PBS). (F) The area of thioS-positive deposits was quantified from 2 sections per mouse in a defined region of interest with a fixed area ($\sim$0.19 mm^2) in sagittal sections of the parietal cortex, dorsal to hippocampus. A significant increase in thioS staining was observed over the course of the study ($q_{47} = 4.9$, $P < .0001$). Treatment with NPT088 significantly reduced thioS staining in parietal cortex ($q_{47} = 2.3$, $P = .045$). N = 19 (Tg-PBS), 18 (Tg-NPT088), 13 (Tg-Time 0). (G) Limb clasping was assessed during week 4 of dosing. rTg4510 mice receiving PBS exhibited significantly more severe limb clasping relative to rTg4510 mice assessed at the beginning of the study ($q_{50} = 2.7$, $P = .02$). Mice treated with NPT088 exhibited a trend for reduced limb clasping ($q_{50} = 1.8$, $P = .13$). N = 20 (Tg-PBS), 20 (Tg-NPT088), 13 (Tg-Time 0). (H) rTg4510 mice that were treated with NPT088 exhibited significantly better performance in the novel object recognition test compared to mice that received PBS ($t = 2$, $df = 21$, $P = .03$). N = 14 (Tg-PBS), 12 (Tg-NPT088). In all panels, asterisks indicate significant difference from Tg-PBS.

Aβ represents a major component of the early pathology associated with AD; however, accumulation of hyperphosphorylated tau-containing NFT pathology appears to be a better correlate of cognitive impairment [48–52]. In AD, tau pathology progresses in a stereotypical manner with first lesions appearing in the locus coeruleus, basal forebrain, and entorhinal cortex from where they appear to spread to the hippocampus and neocortex [53]. There is growing evidence that suggests that this spread of pathology involves escape of tau aggregates from the diseased neurons to the extracellular space, which infects neighboring neurons [54,55]. This mode of cell-to-cell transmission is similar to transmission of misfolded prion protein in transmissible spongiform encephalopathies.

Cell culture models recapitulate the seeding and prion-like transmission by tau aggregates [56]. Preliminary studies from our laboratory show that preformed fibrils made from synthetic peptides of the MTBR region can induce phosphorylation and recruitment of soluble tau into NFT-like aggregates (Supplementary Fig. 2). Furthermore, NPT088 can bind these transmission-competent fibrils with high affinity and remodel them into nonfibrous conformers (Supplementary Fig. 2C). Consistent with these cell culture experiments, we show that NPT088 treatment produces robust efficacy on neuropathologic and functional endpoints in rTg4510 mice (Fig. 5) and can decrease brain atrophy in older rTg4510 mice with severe brain pathology (Fig. 6).

Other studies have demonstrated that passive immunization against p-tau containing epitopes or tau oligomers in AD mouse models significantly reverses tau-related neuropathology and behavioral abnormalities [30,57–65]. Although these results are promising, it has yet to be determined which species of tau (i.e., monomer, oligomer, fibrillar) or which potential p-tau epitopes [66] should be targeted by immunotherapeutic approaches to exhibit significant clinical efficacy. Our data suggest that binding to monomeric tau is unnecessary for efficacy and further suggest that targeting oligomeric and/or fibrous species of tau is sufficient for slowing progression of tauopathy in vivo.

Although it is possible that tau-directed therapeutics will yield significant functional improvement in clinical trials, as suggested by phase II results of a tau aggregation inhibitor [9], no phase III results of the tau immunotherapeutic class have been reported. In AD patients, Aβ and tau pathologies appear to be nonoverlapping, both temporally and anatomically [67,68], suggesting distinct pathologic mechanisms. Moreover, recent studies suggest that extracellular tau increases Aβ production [69] and that in the presence of Aβ pathology, the effect of tau immunotherapies is transient [65]. Therefore, therapeutic approaches that focus on a single pathology may fail to adequately treat AD, especially in more advanced stages of the disease [3]. NPT088 is a single therapeutic candidate that exhibits significant activity on both Aβ and tau, and this activity has been measured both in vitro [14] and in preclinical AD models, which represents a potential advantage for translation of preclinical efficacy.

NPT088 is a unique therapeutic candidate for neurodegenerative disorders that involve accumulation of misfolded protein aggregates. Systemic administration of NPT088 improves cognition, decreases pathologic protein loads, and reduces neuropathology in both Aβ and tau-based transgenic mouse models.

Supplementary data

Supplementary data related to this article can be found at http://dx.doi.org/10.1016/j.trci.2016.06.004.

RESEARCH IN CONTEXT

1. Systematic review: PubMed query ("passive immunization") AND (Abeta OR tau) AND (mouse) NOT (review). Screening of titles and abstracts identified 98 relevant articles. Collectively, findings indicate antibodies reduce pathology and improve cognition only in mouse models that express the specific antigen.
2. Interpretation: Our findings that a fusion protein bivalent for a general amyloid interaction motif (GAIM) reduces pathology and improves cognitive and motor endpoints in transgenic mouse models of either aberrant Aβ or tau accumulation establish GAIM-based therapeutics as a novel strategy targeting misfolded protein aggregates for treatment of Alzheimer's disease.
3. Future directions: Proof-of-concept and proof-of-mechanism studies in patients.

References

[1] Masters CL, Simms G, Weinman NA, Multhaup G, McDonald BL, Beyreuther K. Amyloid plaque core protein in Alzheimer disease and Down syndrome. Proc Natl Acad Sci U S A 1985;82:4245–9.
[2] Goedert M, Spillantini MG, Crowther RA. Tau proteins and neurofibrillary degeneration. Brain Pathol 1991;1:279–86.
[3] Doody RS, Farlow M, Aisen PS. Phase 3 trials of solanezumab and bapineuzumab for Alzheimer's disease. N Engl J Med 2014; 370:1460.
[4] Doody RS, Raman R, Farlow M, Iwatsubo T, Vellas B, Joffe S, et al. A phase 3 trial of semagacestat for treatment of Alzheimer's disease. N Engl J Med 2013;369:341–50.
[5] Doody RS, Thomas RG, Farlow M, Iwatsubo T, Vellas B, Joffe S, et al. Phase 3 trials of solanezumab for mild-to-moderate Alzheimer's disease. N Engl J Med 2014;370:311–21.
[6] Salloway S, Sperling R, Fox NC, Blennow K, Klunk W, Raskind M, et al. Two phase 3 trials of bapineuzumab in mild-to-moderate Alzheimer's disease. N Engl J Med 2014;370:322–33.

[7] Schneider LS, Mangialasche F, Andreasen N, Feldman H, Giacobini E, Jones R, et al. Clinical trials and late-stage drug development for Alzheimer's disease: an appraisal from 1984 to 2014. J Intern Med 2014; 275:251–83.
[8] Wischik C, Staff R. Challenges in the conduct of disease-modifying trials in AD: practical experience from a phase 2 trial of Tau-aggregation inhibitor therapy. J Nutr Health Aging 2009; 13:367–9.
[9] Wischik CM, Bentham P, Wischik DJ, Seng KM. Tau aggregation inhibitor (TAI) therapy with rember™ arrests disease progression in mild and moderate Alzheimer's disease over 50 weeks. Alzheimers Dement 2008;4:T167.
[10] Demattos RB, Lu J, Tang Y, Racke MM, Delong CA, Tzaferis JA, et al. A plaque-specific antibody clears existing beta-amyloid plaques in Alzheimer's disease mice. Neuron 2012;76:908–20.
[11] Wisniewski T, Goni F. Immunotherapy for Alzheimer's disease. Biochem Pharmacol 2014;88:499–507.
[12] Sevigny J. Aducanumab (BIIB037), an Anti-Amyloid Beta Monoclonal Antibody, in Patients with Prodromal or Mild Alzheimer's Disease: Interim Results of a Randomized, Double-Blind, Placebo-Controlled, Phase 1B Study. Alzheimer's Association International Conference. Washington DC: Alzheimer's Association; 2015.
[13] Solomon B, Goren O. Method and filamentous phage for treating inflammation associated with amyloid deposits and brain inflammation involving activated microglia. In: USPTO, editor. United States: Ramot at Tel-Aviv University Ltd. (Tel-Aviv, IL); 2013.
[14] Krishnan R, Tsubery H, Proschitsky MY, Asp E, Lulu M, Gilead S, et al. A Bacteriophage Capsid Protein Provides a General Amyloid Interaction Motif (GAIM) That Binds and Remodels Misfolded Protein Assemblies. J Mol Biol 2014;426:2500–19.
[15] Lambert MP, Barlow AK, Chromy BA, Edwards C, Freed R, Liosatos M, et al. Diffusible, nonfibrillar ligands derived from Abeta1-42 are potent central nervous system neurotoxins. Proc Natl Acad Sci U S A 1998;95:6448–53.
[16] Hsiao K, Chapman P, Nilsen S, Eckman C, Harigaya Y, Younkin S, et al. Correlative memory deficits, Abeta elevation, and amyloid plaques in transgenic mice. Science 1996;274:99–102.
[17] Santacruz K, Lewis J, Spires T, Paulson J, Kotilinek L, Ingelsson M, et al. Tau suppression in a neurodegenerative mouse model improves memory function. Science 2005;309:476–81.
[18] Bohrmann B, Baumann K, Benz J, Gerber F, Huber W, Knoflach F, et al. Gantenerumab: a novel human anti-Abeta antibody demonstrates sustained cerebral amyloid-beta binding and elicits cell-mediated removal of human amyloid-beta. J Alzheimers Dis 2012;28:49–69.
[19] Waldmann H, Adams E, Cobbold S. Reprogramming the immune system: co-receptor blockade as a paradigm for harnessing tolerance mechanisms. Immunol Rev 2008;223:361–70.
[20] Shankar GM, Welzel AT, McDonald JM, Selkoe DJ, Walsh DM. Isolation of low-n amyloid beta-protein oligomers from cultured cells, CSF, and brain. Methods Mol Biol 2011;670:33–44.
[21] Larson ME, Lesne SE. Soluble Abeta oligomer production and toxicity. J Neurochem 2012;120:125–39.
[22] Carroll JC, Iba M, Bangasser DA, Valentino RJ, James MJ, Brunden KR, et al. Chronic stress exacerbates tau pathology, neurodegeneration, and cognitive performance through a corticotropin-releasing factor receptor-dependent mechanism in a transgenic mouse model of tauopathy. J Neurosci 2011;31:14436–49.
[23] Brouillette J, Caillierez R, Zommer N, Alves-Pires C, Benilova I, Blum D, et al. Neurotoxicity and memory deficits induced by soluble low-molecular-weight amyloid-beta1-42 oligomers are revealed in vivo by using a novel animal model. J Neurosci 2012;32:7852–61.
[24] Walsh DM, Klyubin I, Fadeeva JV, Cullen WK, Anwyl R, Wolfe MS, et al. Naturally secreted oligomers of amyloid beta protein potently inhibit hippocampal long-term potentiation in vivo. Nature 2002; 416:535–9.
[25] Wang HW, Pasternak JF, Kuo H, Ristic H, Lambert MP, Chromy B, et al. Soluble oligomers of beta amyloid (1-42) inhibit long-term potentiation but not long-term depression in rat dentate gyrus. Brain Res 2002;924:133–40.
[26] Glabe C. Intracellular mechanisms of amyloid accumulation and pathogenesis in Alzheimer's disease. J Mol Neurosci 2001;17:137–45.
[27] Taglialatela G, Hogan D, Zhang WR, Dineley KT. Intermediate- and long-term recognition memory deficits in Tg2576 mice are reversed with acute calcineurin inhibition. Behav Brain Res 2009; 200:95–9.
[28] Chapman PF, White GL, Jones MW, Cooper-Blacketer D, Marshall VJ, Irizarry M, et al. Impaired synaptic plasticity and learning in aged amyloid precursor protein transgenic mice. Nat Neurosci 1999;2:271–6.
[29] Kawarabayashi T, Younkin LH, Saido TC, Shoji M, Ashe KH, Younkin SG. Age-dependent changes in brain, CSF, and plasma amyloid (beta) protein in the Tg2576 transgenic mouse model of Alzheimer's disease. J Neurosci 2001;21:372–81.
[30] Sankaranarayanan S, Barten DM, Vana L, Devidze N, Yang L, Cadelina G, et al. Passive immunization with phospho-tau antibodies reduces tau pathology and functional deficits in two distinct mouse tauopathy models. PLoS One 2015;10:e0125614.
[31] Ramsden M, Kotilinek L, Forster C, Paulson J, McGowan E, SantaCruz K, et al. Age-dependent neurofibrillary tangle formation, neuron loss, and memory impairment in a mouse model of human tauopathy (P301L). J Neurosci 2005;25:10637–47.
[32] Lalonde R, Strazielle C. Brain regions and genes affecting limb-clasping responses. Brain Res Rev 2011;67:252–9.
[33] Yoshiyama Y, Higuchi M, Zhang B, Huang SM, Iwata N, Saido TC, et al. Synapse loss and microglial activation precede tangles in a P301S tauopathy mouse model. Neuron 2007;53:337–51.
[34] Ishihara T, Higuchi M, Zhang B, Yoshiyama Y, Hong M, Trojanowski JQ, et al. Attenuated neurodegenerative disease phenotype in tau transgenic mouse lacking neurofilaments. J Neurosci 2001;21:6026–35.
[35] Terwel D, Lasrado R, Snauwaert J, Vandeweert E, Van Haesendonck C, Borghgraef P, et al. Changed conformation of mutant Tau-P301L underlies the moribund tauopathy, absent in progressive, nonlethal axonopathy of Tau-4R/2N transgenic mice. J Biol Chem 2005;280:3963–73.
[36] Newell KL, Hyman BT, Growdon JH, Hedley-Whyte ET. Application of the National Institute on Aging (NIA)-Reagan Institute criteria for the neuropathological diagnosis of Alzheimer disease. J Neuropathol Exp Neurol 1999;58:1147–55.
[37] Glenner GG, Wong CW. Alzheimer's disease and Down's syndrome: sharing of a unique cerebrovascular amyloid fibril protein. Biochem Biophys Res Commun 1984;122:1131–5.
[38] McLean CA, Cherny RA, Fraser FW, Fuller SJ, Smith MJ, Beyreuther K, et al. Soluble pool of Abeta amyloid as a determinant of severity of neurodegeneration in Alzheimer's disease. Ann Neurol 1999;46:860–6.
[39] Levites Y, Das P, Price RW, Rochette MJ, Kostura LA, McGowan EM, et al. Anti-Abeta42- and anti-Abeta40-specific mAbs attenuate amyloid deposition in an Alzheimer disease mouse model. J Clin Invest 2006;116:193–201.
[40] Das P, Murphy MP, Younkin LH, Younkin SG, Golde TE. Reduced effectiveness of Abeta1-42 immunization in APP transgenic mice with significant amyloid deposition. Neurobiol Aging 2001; 22:721–7.
[41] Wang A, Das P, Switzer RC 3rd, Golde TE, Jankowsky JL. Robust amyloid clearance in a mouse model of Alzheimer's disease provides novel insights into the mechanism of amyloid-beta immunotherapy. J Neurosci 2011;31:4124–36.
[42] Haupt C, Bereza M, Kumar ST, Kieninger B, Morgado I, Hortschansky P, et al. Pattern recognition with a fibril-specific antibody fragment reveals the surface variability of natural amyloid fibrils. J Mol Biol 2011;408:529–40.
[43] Wilcock DM, Rojiani A, Rosenthal A, Levkowitz G, Subbarao S, Alamed J, et al. Passive amyloid immunotherapy clears amyloid and

transiently activates microglia in a transgenic mouse model of amyloid deposition. J Neurosci 2004;24:6144–51.
[44] DeMattos RB, Bales KR, Cummins DJ, Dodart JC, Paul SM, Holtzman DM. Peripheral anti-A beta antibody alters CNS and plasma A beta clearance and decreases brain A beta burden in a mouse model of Alzheimer's disease. Proc Natl Acad Sci U S A 2001;98:8850–5.
[45] Siemers ER, Friedrich S, Dean RA, Gonzales CR, Farlow MR, Paul SM, et al. Safety and changes in plasma and cerebrospinal fluid amyloid beta after a single administration of an amyloid beta monoclonal antibody in subjects with Alzheimer disease. Clin Neuropharmacol 2010;33:67–73.
[46] Farlow M, Arnold SE, van Dyck CH, Aisen PS, Snider BJ, Porsteinsson AP, et al. Safety and biomarker effects of solanezumab in patients with Alzheimer's disease. Alzheimers Dement 2012;8:261–71.
[47] Andreasen N, Simeoni M, Ostlund H, Lisjo PI, Fladby T, Loercher AE, et al. First administration of the Fc-attenuated anti-beta amyloid antibody GSK933776 to patients with mild Alzheimer's disease: a randomized, placebo-controlled study. PLoS One 2015;10:e0098153.
[48] Duyckaerts C, Brion JP, Hauw JJ, Flament-Durand J. Quantitative assessment of the density of neurofibrillary tangles and senile plaques in senile dementia of the Alzheimer type. Comparison of immunocytochemistry with a specific antibody and Bodian's protargol method. Acta Neuropathol 1987;73:167–70.
[49] Duyckaerts C, Delaere P, Hauw JJ, Abbamondi-Pinto AL, Sorbi S, Allen I, et al. Rating of the lesions in senile dementia of the Alzheimer type: concordance between laboratories. A European multicenter study under the auspices of EURAGE. J Neurol Sci 1990;97:295–323.
[50] Delaere P, Duyckaerts C, Brion JP, Poulain V, Hauw JJ. Tau, paired helical filaments and amyloid in the neocortex: a morphometric study of 15 cases with graded intellectual status in aging and senile dementia of Alzheimer type. Acta Neuropathol 1989;77:645–53.
[51] Arriagada PV, Growdon JH, Hedley-Whyte ET, Hyman BT. Neurofibrillary tangles but not senile plaques parallel duration and severity of Alzheimer's disease. Neurology 1992;42:631–9.
[52] Dickson DW. Neuropathological diagnosis of Alzheimer's disease: a perspective from longitudinal clinicopathological studies. Neurobiol Aging 1997;18:S21–6.
[53] Braak H, Braak E. Neuropathological stageing of Alzheimer-related changes. Acta Neuropathol 1991;82:239–59.
[54] Clavaguera F, Bolmont T, Crowther RA, Abramowski D, Frank S, Probst A, et al. Transmission and spreading of tauopathy in transgenic mouse brain. Nat Cell Biol 2009;11:909–13.
[55] Iba M, Guo JL, McBride JD, Zhang B, Trojanowski JQ, Lee VM. Synthetic tau fibrils mediate transmission of neurofibrillary tangles in a transgenic mouse model of Alzheimer's-like tauopathy. J Neurosci 2013;33:1024–37.
[56] Guo JL, Lee VM. Seeding of normal Tau by pathological Tau conformers drives pathogenesis of Alzheimer-like tangles. J Biol Chem 2011;286:15317–31.
[57] Yanamandra K, Kfoury N, Jiang H, Mahan TE, Ma S, Maloney SE, et al. Anti-tau antibodies that block tau aggregate seeding in vitro markedly decrease pathology and improve cognition in vivo. Neuron 2013;80:402–14.
[58] Boutajangout A, Ingadottir J, Davies P, Sigurdsson EM. Passive immunization targeting pathological phospho-tau protein in a mouse model reduces functional decline and clears tau aggregates from the brain. J Neurochem 2011;118:658–67.
[59] Boutajangout A, Quartermain D, Sigurdsson EM. Immunotherapy targeting pathological tau prevents cognitive decline in a new tangle mouse model. J Neurosci 2010;30:16559–66.
[60] Theunis C, Crespo-Biel N, Gafner V, Pihlgren M, Lopez-Deber MP, Reis P, et al. Efficacy and safety of a liposome-based vaccine against protein Tau, assessed in tau.P301L mice that model tauopathy. PLoS One 2013;8:e72301.
[61] Troquier L, Caillierez R, Burnouf S, Fernandez-Gomez FJ, Grosjean ME, Zommer N, et al. Targeting phospho-Ser422 by active Tau Immunotherapy in the THYTau22 mouse model: a suitable therapeutic approach. Curr Alzheimer Res 2012;9:397–405.
[62] Chai X, Wu S, Murray TK, Kinley R, Cella CV, Sims H, et al. Passive immunization with anti-Tau antibodies in two transgenic models: reduction of Tau pathology and delay of disease progression. J Biol Chem 2011;286:34457–67.
[63] Castillo-Carranza DL, Gerson JE, Sengupta U, Guerrero-Munoz MJ, Lasagna-Reeves CA, Kayed R. Specific targeting of tau oligomers in htau mice prevents cognitive impairment and tau toxicity following injection with brain-derived tau oligomeric seeds. J Alzheimers Dis 2014;40:S97–111.
[64] Castillo-Carranza DL, Sengupta U, Guerrero-Munoz MJ, Lasagna-Reeves CA, Gerson JE, Singh G, et al. Passive immunization with Tau oligomer monoclonal antibody reverses tauopathy phenotypes without affecting hyperphosphorylated neurofibrillary tangles. J Neurosci 2014;34:4260–72.
[65] Walls KC, Ager RR, Vasilevko V, Cheng D, Medeiros R, LaFerla FM. p-Tau immunotherapy reduces soluble and insoluble tau in aged 3xTg-AD mice. Neurosci Lett 2014;575:96–100.
[66] d'Abramo C, Acker CM, Jimenez H, Davies P. Passive Immunization in JNPL3 Transgenic Mice Using an Array of Phospho-Tau Specific Antibodies. PLoS One 2015;10:e0135774.
[67] Delacourte A, Sergeant N, Champain D, Wattez A, Maurage CA, Lebert F, et al. Nonoverlapping but synergetic tau and APP pathologies in sporadic Alzheimer's disease. Neurology 2002;59:398–407.
[68] Jack CR Jr, Knopman DS, Jagust WJ, Shaw LM, Aisen PS, Weiner MW, et al. Hypothetical model of dynamic biomarkers of the Alzheimer's pathological cascade. Lancet Neurol 2010;9:119–28.
[69] Bright J, Hussain S, Dang V, Wright S, Cooper B, Byun T, et al. Human secreted tau increases amyloid-beta production. Neurobiol Aging 2015;36:693–709.
[70] Luna LG. Manual of Histologic Staining Methods of the Armed Forces Institute of Pathology. 3rd ed. New York: Blakiston Division, McGraw Hill; 1968.
[71] Berger Z, Roder H, Hanna A, Carlson A, Rangachari V, Yue M, et al. Accumulation of pathological tau species and memory loss in a conditional model of tauopathy. J Neurosci 2007;27:3650–62.
[72] Sahara N, DeTure M, Ren Y, Ebrahim AS, Kang D, Knight J, et al. Characteristics of TBS-extractable hyperphosphorylated tau species: aggregation intermediates in rTg4510 mouse brain. J Alzheimers Dis 2013;33:249–63.